

# Seismogenic Structure of the 1605 Qiongsan $M7\frac{1}{2}$ Earthquake and Its Holocene Activity History in Northern Hainan Island, China: Evidence from Cross-Section Drilling and Shallow Seismic Profile

Chaoqun Wang<sup>#1, 2, 3</sup>, Liyun Jia<sup>#\*1, 2, 4</sup>, Daogong Hu<sup>1, 2</sup>, Shibiao Bai<sup>5</sup>, Zhengwang Hu<sup>6</sup>,  
Dongxia Sun<sup>1, 2</sup>, Xiaoxiao Yang<sup>1, 2</sup>, Lei Zhang<sup>1, 2</sup>, Xiumin Ma<sup>1, 4</sup>

1. Institute of Geomechanics, Chinese Academy of Geological Sciences, Beijing 100081, China



2. Key Laboratory of Active Tectonics and Geological Safety, Ministry of Natural Resources, Beijing 100081, China

3. Key Laboratory of Geohazard Prevention of Hilly Mountains, Ministry of Land and Resources (Fujian Key Laboratory of Geohazard Prevention), Fuzhou 350002, China

4. Observation and Research Station of Crustal Stress and Strain in Beijing, Ministry of Natural Resources, Beijing 100081, China

5. College of Marine Science and Engineering, Nanjing Normal University, Nanjing 210023, China

6. Hubei Subsurface Multi-Scale Imaging Key Laboratory, School of Geophysics and Geomatics, China University of Geosciences, Wuhan 430074, China

 Chaoqun Wang: <https://orcid.org/0000-0001-8866-2161>;  Liyun Jia: <https://orcid.org/0000-0001-8273-3301>

**ABSTRACT:** The 1605  $M7\frac{1}{2}$  Earthquake is the only earthquake in the history of China that has caused large-scale land subsidence into the sea, with the total area of land subsidence exceeding 100 km<sup>2</sup>. The disaster has led to the sinking of 72 villages. There is still no clear understanding of the source seismogenic fault of this earthquake. In this work, we conducted a detailed study of the middle segment of the Maniao-Puqian fault (MPF), which is the epicenter area, through geomorphological survey, data collection, shallow seismic exploration, cross-section drilling, and chronological dating. The results showed that the middle segment of the MPF zone is composed of three nearly parallel normal faults with a dextral strike-slip: “Macun-Luodou fault (F2-1), Haixiu-Dongyuan fault (F2-2), and Changliu-Zhuxihe fault (F2-3)”. And F2-2 is composed of two secondary faults, namely F2-2' and F2-2'', with a flower-shaped structure buried under the ground. It is distributed nearly east-west, dipping to the north and has experienced at least five stages of activities since the Miocene. The vertical activity rates of F2-2' and F2-2'' are ~2.32 and ~2.5 mm/a, since the Holocene, respectively. There were eight cycles of transgression and regression since the Miocene. The fault activity resulted in the thickening of the Holocene strata with a slight dip to the south, on the hanging wall, showing V-shaped characteristics. The MPF is likely the source seismogenic fault of the  $M7\frac{1}{2}$  earthquake that hit Qiongsan in 1605.

**KEY WORDS:** seismogenic structure, earthquakes, Maniao-Puqian fault, fault activity history, geomorphology.

## 0 INTRODUCTION

The Northern Hainan Island, located at the junction of the South China Plate, Indochina Plate, and Philippine Plate, contains widely developed active faults and Quaternary volcanoes (e. g., Liu Y et al., 2020; Hu D G et al., 2019; Hu Y X et al., 2016; Liu H et al., 2008; Fan et al., 2004). Earthquakes have fre-

quently hit this area since the Cenozoic due to plate interaction and deep magmatic activity. On July 13, 1605, the Qiongsan  $M7\frac{1}{2}$  Earthquake, the most destructive earthquake in the history of South China, hit the northern Hainan Island. It is the only earthquake in the history of China that has caused large-scale land subsidence into the sea (Chen and Huang, 1989, 1979; Xu, 1986a, b, c, 1985; Xu et al., 1982). Four aftershocks with magnitudes ranging from  $M6$  to  $M6\frac{1}{2}$  occurred in just half a year following the earthquake (Ren and He, 2006), with the extreme seismic intensity reaching XI degree. Hence, the seismogenic structure of this earthquake and the active faults in northern Hainan Island area have received extensive attention (Liu H G et al., 2018; Xu X W, 2015; Xu Q H, 2007, 1986a, b, c, 1985; Li et al., 2006; Chen and Huang, 1989, 1979; Xu et al., 1982).

\*Corresponding author: 158943653@qq.com

# These authors contributed equally to this article

© China University of Geosciences (Wuhan) and Springer-Verlag GmbH Germany, Part of Springer Nature 2024

Manuscript received August 5, 2021.

Manuscript accepted November 17, 2021.

Wang Chaoqun, Jia Liyun, Hu Daogong, Bai Shibiao, Hu Zhengwang, Sun Dongxia, Yang Xiaoxiao, Zhang Lei, Ma Xiumin, 2024. Seismogenic Structure of the 1605 Qiongsan  $M7\frac{1}{2}$  Earthquake and Its Holocene Activity History in Northern Hainan Island, China: Evidence from Cross-Section Drilling and Shallow Seismic Profile. *Journal of Earth Science*, 35(3): 905–917. <https://doi.org/10.1007/s12583-021-1585-x>. <http://en.earth-science.net>

However, since the epicenter of the earthquake is located in a coastal plain area, and the faults are mostly buried; therefore, the seismogenic structure remains controversial. Xu (1985) concluded that the 1605 Qiongsan Earthquake was the result of the activity of the NW-trending fault (F13: Puqian-Qinglan fault (PQF), Figure 1) based on the intensity of historical earthquakes, and the subsidence of the Dongzhai Port was found to be as high as 10 m. According to other scholars, the seismic-controlling structure of the Qiongsan  $M7\frac{1}{2}$  Earthquake is the high-angle translation normal fault (Figure 1) formed by the intersection of the “X” type Maniao-Puqian fault (MPF) (F2) (Figure 1) and the PQF, with the former playing a major role (Xu, 2007; Chen and Huang, 1989, 1979). Many studies have been conducted on the deep occurrence, geometric distribution, and active age of the MPF (Wang et al., 2021; Li W et al., 2019; Liu F X et al., 2018; Liu H G et al., 2018; Li P et al., 1988). However, stratigraphic division is the basis for judging whether faults are active or not. The Quaternary strata in the northern Hainan Island are complex (Geological Survey Institute of Hainan Province, 2019). There are not only continental deposits formed by lake deposits and river erosion, but also a large number of marine deposits as well as volcanic rocks with multiple periods and cycles. Because of the lack of carding of the standard strata in the fault zone, the fault activity cannot be accurately judged, particularly in the middle segment of the fault. Therefore, clarifying the stratigraphic sequence, age, and sedimentary evolution of the fault zone and finding the symbolic stable strata are the basis for judging the fault activity.

In this study, we recovered the sedimentary evolution process of the middle segment of the MPF, presenting new evidence that demonstrates the Holocene activity of the active faults. We inverted the fault activity history since the Miocene and analyzed the seismogenic structure in the middle segment of the MPF zone and its controlling effect on the 1605 Qiongsan  $M7\frac{1}{2}$  Earthquake. The results provide a better understanding of the crustal stability of the northern Hainan Island and the formation and evolution of the Qiongzhou Strait and Dongzhai Port.

## 1 MANIAO-PUQIAN FAULT ZONE

The Maniao-Puqian fault zone lies in the northern part of Hainan Island, southern China, located at the border of the South China Plate, Indochina Plate, and Philippine Plate (Figure 1). Since the Paleozoic, this area has experienced convergence and separation of the microplates of the Paleo-Tethys and Pacific tectonic domains multiple times, resulting in the formation of multiple suture zones and deep and large fractures of the lithosphere, separating the different blocks therein (Chen et al., 2024; Li et al., 2024; Zhou et al., 2023; Peng et al., 2022; Zhao et al., 2016; Zhang G W et al., 2013; Zhang Y M et al., 1997). In the Cenozoic, with the interaction between the plates and under the background of deep magmatic activity, tectonic activities were active, there were many active faults, and Quaternary volcanic development was extensive (Li et al., 2012; Jia et al., 2006; Huang and Cai, 1994). A series of faults striking along NE, EW, and NW developed, playing an important role in the regional geomorphic evolution; these faults threaten

major projects and the safety of urban construction in the area (Hu et al., 2019).

The stratigraphic system in the MPF zone is complex. The basement strata are the Silurian Konglicun Formation ( $S_1k$ ), Tulliecun formation ( $S_1t$ ) metamorphic rocks, and Triassic granite. The Cenozoic strata mainly consist of sedimentary rocks and volcanics. The volcanics are dominated by the Middle Pleistocene Duowen Formation basalt ( $Qp^2d$ ), the upper part of which is mostly weathered by approximately 2 m-thick basalts of the Daotang Formation ( $Qp^3d$ ) of the Upper Pleistocene and Shishan Formation ( $Qh^1$ ). Sedimentary rocks mainly include Miocene Jiaowei Formation sandstone, mudstone ( $N_1j$ ), Dengloujiao Formation sandstone ( $N_1d$ ), and Pliocene Haikou Formation shell conglomerate, sandstone, and mudstone ( $N_2h$ ). Based on the classical stratigraphic section of this area, the Quaternary has been divided from bottom to top as follows: Xiuying Formation ( $Qp^1x$ ) clay and fine sands of the Lower Pleistocene, Beihai Formation ( $Qp^2b$ ) glutenite of the Middle Pleistocene, Basuo Formation ( $Qp^3bs$ ) sands, and Yandun Formation ( $Qh^1y$ ) of the Holocene (Geological Survey Institute of Hainan Province, 2019; Xia et al., 2019; Long et al., 2006; Xue, 1983; Wang, 1981).

In the 1980s, the MPF zone was discovered through geophysical exploration, such as gravity, magnetism, and artificial earthquake analyses, and the MPF was considered a large-scale deep fault penetrating the crust (Chen and Huang, 1989; Ding, 1988; Li et al., 1988; Lin et al., 1988; Sun and Yan, 1988; Yang et al., 1988). Evident sectional characteristics were observed for three segments bounded by Maiao, Qiongsan, and Dongzhai Port (Wang et al., 2021; Li et al., 1988). The deep occurrence of the three segments was found to be inconsistent. The middle and western segments are northern-dipping normal faults, while the eastern segment is southward-dipping normal faults (Li et al., 1988). Recently, we found that the eastern segment of this fault is composed of eight north-dipping or south-dipping NEE-trending normal faults, constituting a three grabens and two barriers structure. We confirmed its frequent activation during the Holocene (Wang et al., 2021). Meanwhile, through tectonic geomorphic investigation, our team found geological evidence of multiple activities of the fault zone since the Late Pleistocene in the volcanic-sedimentary rocks of the Chengmai-Laocheng area in the western section (Li et al., 2019). In addition, in the middle section of the fault zone, the drillings exposed the fault slickenside of the Maniao-Puqian fault activity that occurred in the Pliocene conch conglomerate and mudstone of Haikou Formation in the north of Cangtuo Village and the east of Guida Road (Figure 2a) (Hu et al., 2019). Xu (2015) obtained the spatial distribution characteristics of the segment of Macun Country to Cangxi Country for the east-west segment. They believed that this segment is an east-west-oriented normal fault, with a steep angle, and the age of the latest stratigraphic stratum by faulting was found to be more than 48 000 years. Liu H G et al. (2018) considered that the four branch faults of Taolancun in the middle segment of the MPF were active in the Holocene based on a combined drilling profile exploration. The buried depth of the top fault point was found to be in the range of 9.2–10.5 m, and the cumulative displacement during the Quaternary was in the range of 1–2 m.

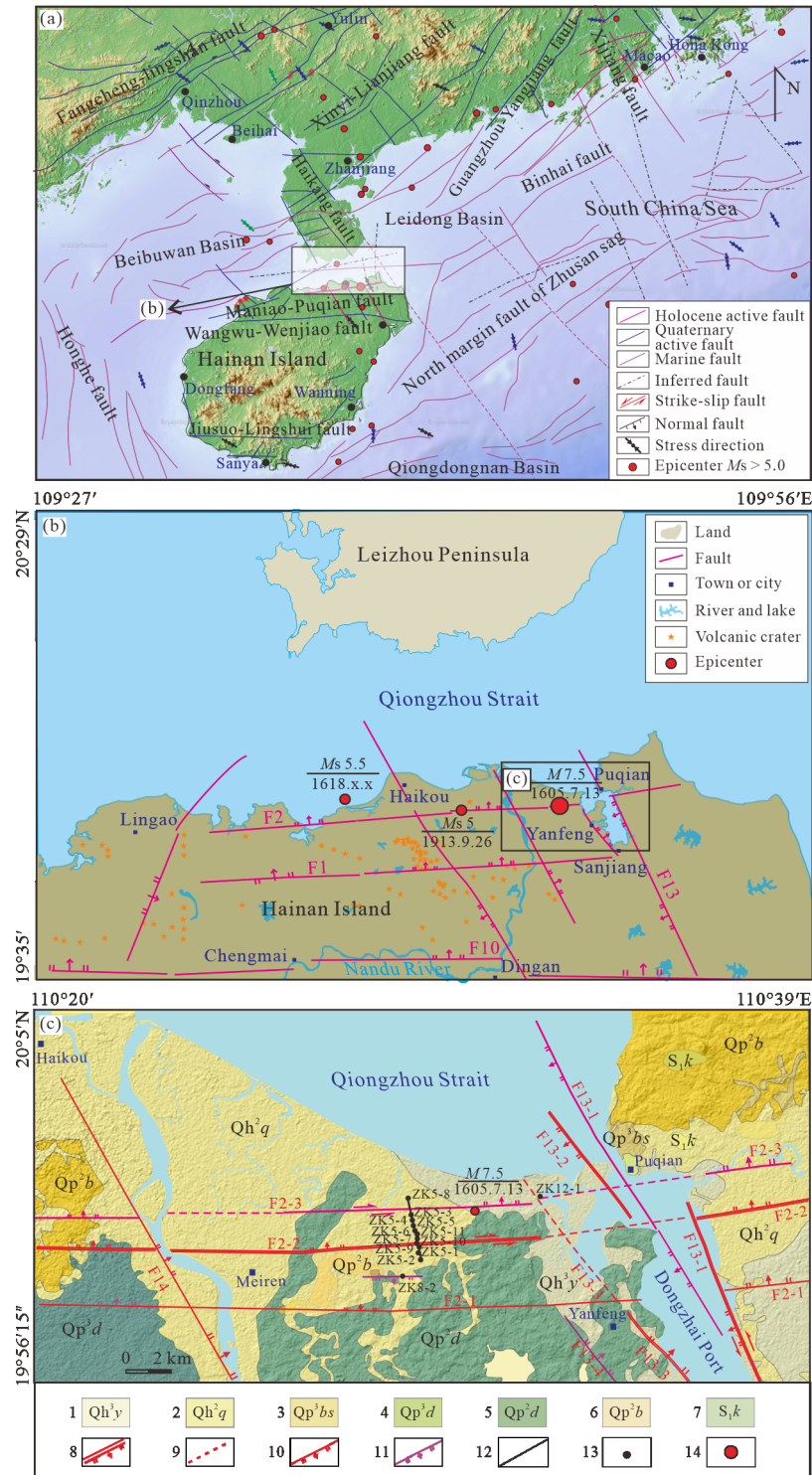


**Figure 1.** Active faults distribution map of the research area. 1. Yandun Formation in the Holocene; 2. Qiongsan Formation in the Holocene; 3. Basuo Formation in the Late Pleistocene; 4. Daotang Formation in the Late Pleistocene; 5. Duowen Formation in the Middle Pleistocene; 6. Beihai Formation in the Middle Pleistocene; 7. Kongliecun Formation in the Silurian; 8. Holocene active fault; 9. Holocene buried fault; 10. Late Pleistocene active fault; 11. Early–Middle Pleistocene active fault (the codes of faults continue to use the predecessors of the entire northern Hainan Island numbering; Hu et al., 2019; Xu, 2015); 12. drill hole section line; 13. drill hole; 14. epicenter; F1. Ruguancun-Yunlong fault; F2. Maniao-Puqian fault; F10. Wangwu-Wenjiao fault; F13. Puqian-Qinglan fault.

**2 RESEARCH METHODS**

**2.1 Geological and Geomorphological Survey and Data Collection**

Geological and geomorphic survey is the basis for studying fault activities. Combined with remote sensing image inter-

pretation, we made a detailed field survey on the geological and geomorphic conditions of the MPF zone. In addition, we collected a large amount of geophysical and drilling data in the study area, given the lack of outcrops in the area.



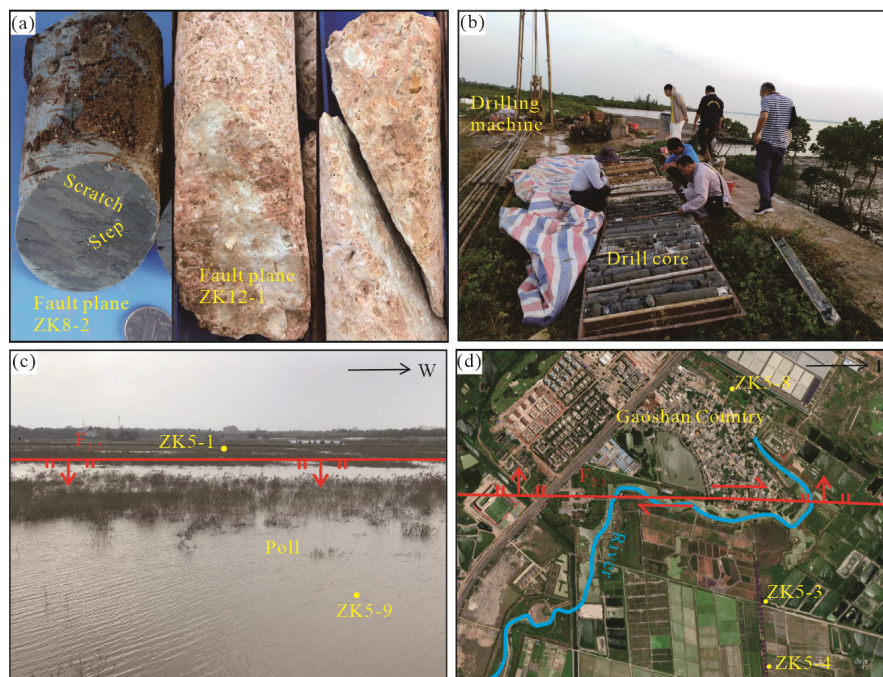


**Figure 2.** Drillings and geomorphology of the MPF zone. (a) Fault slickenside of ZK8-2 and ZK12-1; (b) drilling construction; (c) pool landform formed by a normal fault; (d) drainage deflection by strike-slip faulting.

## 2.2 Shallow Seismic Exploration

Based on the geological and geomorphic survey and data analysis, the approximate distribution location of the MPF was speculated. Subsequently, we laid out shallow seismic detection lines across the fault (Figure 1). The starting point coordinates and the end point coordinates of the detection line are  $19^{\circ}59'26''\text{N}$ ,  $110^{\circ}29'20''\text{E}$  and  $20^{\circ}0'18''\text{N}$ ,  $110^{\circ}29'14''\text{E}$ . A drop-weight hammer weighing 326 kg, height 7 m as the earthquake source and an intermediate excitation observation system were used in the detection process. The acquisition parameters were determined by field testing. The channel spacing was 5 m, the shot spacing was 20 m, and the sampling interval was 0.5 ms. After signal acquisition, a series of digital processing steps, such as eliminating the interference and observing the influence of system parameters, were conducted to obtain a clear seismic profile with a high signal-to-noise ratio, which could be used to detect the extension of deep faults.

## 2.3 Drilling Construction and Cataloging

The specific location and activities of buried faults can be determined by rows of drillings across a fault. We drilled 12 geological holes and termed them ZK5-1 to ZK5-12. The position and elevation of these drillings are shown in Table 1. We used a mechanical drilling machine to drill to a depth of  $\sim 100$  m, the deviation of the borehole slope was  $<1^{\circ}$ , the core diameter was  $>91$  mm, and a detailed catalog of these drillings was made.

## 2.4 Chronological Dating

To determine the age of the landmark strata and the amplitude of the fault activities, the  $\text{AMS}^{14}\text{C}$  dating method was used for the upper carbon-bearing sediments and shells. Optically stimulated luminescence (OSL) dating was performed on sediments obtained from strata predicted to be older than 50 000

**Table 1** Drillings position and elevation

Drilling No.	Longitude	Latitude	Elevation (m)
ZK5-2	$110^{\circ}29'20.96''\text{E}$	$19^{\circ}59'276''\text{N}$	2.091
ZK5-1	$110^{\circ}29'206''\text{E}$	$19^{\circ}59'34''\text{N}$	2.258
ZK5-9	$110^{\circ}29'20''\text{E}$	$19^{\circ}59'37''\text{N}$	1.960
ZK5-10	$110^{\circ}29'20''\text{E}$	$19^{\circ}59'38''\text{N}$	2.280
ZK5-7	$110^{\circ}29'20''\text{E}$	$19^{\circ}59'38''\text{N}$	2.108
ZK5-11	$110^{\circ}29'20''\text{E}$	$19^{\circ}59'39''\text{N}$	1.997
ZK5-6	$110^{\circ}29'18''\text{E}$	$19^{\circ}59'42''\text{N}$	2.714
ZK5-5	$110^{\circ}29'18''\text{E}$	$19^{\circ}59'46''\text{N}$	3.022
ZK5-4	$110^{\circ}29'17''\text{E}$	$19^{\circ}59'58''\text{N}$	2.440
ZK5-3	$110^{\circ}29'16''\text{E}$	$20^{\circ}00'08''\text{N}$	3.510
ZK5-8	$110^{\circ}29'11''\text{E}$	$20^{\circ}03'72''\text{N}$	2.629

years. Samples were collected based on laboratory requirements, and the Neogene and Paleogene sediments were mainly inferred by the correlation with regional stratigraphic results based on the ages of predecessors. The OSL dating samples were tested in the optically stimulated luminescence (OSL) laboratory of Nanjing Normal University for completion, and the  $^{14}\text{C}$  samples were sent to Bata Laboratory, United States, for completion.

## 3 RESULTS

### 3.1 Geomorphological Characteristics of the MPF Zone

Through detailed geological and geomorphic investigations, the topography in the middle segment of the MPF zone was found to be relatively flat; however, the landforms on both sides of the fault zone were quite different: the north bank of the fault zone is mainly composed of Marine plain and



river alluvial delta, the west of the south bank of the fault zone is composed of Nandu River delta, and the east of the fault zone is composed of volcanic laterite platform and lagoon plain (Figure 1c). On detecting the profile line in Gaoshan Village, the topography to the north of ZK5-1 on the hanging wall was evidently low, which led to the formation of a depression pool in the falling part of the hanging wall during flood season (Figure 2c). In addition, the remote sensing image clearly showed that the river turns nearly  $90^\circ$  right on the fault line (Figure 2d), which should be related to the dextral strike slip of the fault.

### 3.2 Shallow Seismic Detection Results and Analysis

After the acquisition and processing of the shallow seismic data of S142, the shallow seismic profile was obtained (Figure 3). There are four groups of in-phase axes of reflected waves, which have strong amplitude and good continuity and can be traced continuously. The first reflection has evident in-phase axis (T0), strong amplitude, and good continuity; based on the drilling results, this is supposed to be the boundary between the Quaternary strata (Q) and Pliocene Haikou Formation ( $N_2h$ ). It is clearly shown that the in-phase axis (T0) was incontinuous and tilted near the fault zone (between the ZK5-1 and ZK5-6). This could be interpreted as the fractured formation near the fault zone. The second reflection phase axis (T1) is inferred to be the interface between the Pliocene Haikou Formation ( $N_2h$ ) and the Miocene ( $N_1$ ); in other words, it is the bottom boundary of the Haikou Formation ( $N_2h$ ). The third reflection in phase (T2) is inferred as the Miocene ( $N_1$ ) inner layer interface. The fourth reflection phase axis (T3) indicates the boundary between the Miocene strata and the Silurian (S) metamorphic rocks. The thickness of the Quaternary system is approximately 10 m, and the minimum and maximum elevations of its floor are -25 and -15 m, respectively. The average thickness of Haikou Formation is approximately 90 m, and the minimum elevation, maximum elevation, and average elevation of its floor are -120, -85, and -102 m, respectively.

Based on the marked strata dislocation in the seismic profile (S142) and the drilling records (Hu et al., 2019), it can be inferred that the two faults F2-2' and F2-2'' at the bottom interface of Haikou Formation have a small vertical fault distance and sectional wave characteristics. It extends down to the fault F2-2. The overall dip of the fault is NNW, the apparent dip is approximately  $70^\circ$ , and the vertical fault distance is approxi-

mately 20 m by the T3 boundary.

### 3.3 Sedimentary and Tectonic Characteristics of the MPF Zone Strata Revealed by Drillings

The 12 drillings with a depth of approximately 100 m helped reveal the strata since the Miocene. Based on the lithologic characteristics of each set of strata, the strata can be divided into five units from top to bottom, among which unit 2 and unit 4 for judging the fault activity and environmental evolution can be divided into 5 and 6 subunits, respectively. Figure 4 shows the lithologic characteristics of each unit.

Unit 1: Light grayish-brown-yellow clayey fine sand, medium fine sand. It belongs to Holocene Qiongsan Formation (Qhq), 0.6–2.3 m thick.

Unit 2: A set of grayish, caesious sandy clay, local gravel, enriched marine shell fossils. It belongs to Holocene Qiongsan Formation (Qhq). Based on the detailed lithology and sedimentary environment, it can be divided into the following five subunits.

Unit 2-1: In this unit, ZK5-9 and ZK5-10 are dark gray-light gray silty clays, which gradually coarsen to ZK5-7 and ZK5-11 and transition to a dark gray clayey medium fine sand. ZK5-6, ZK5-5, ZK5-4, and ZK5-3 transition to medium coarse sand containing pebbles, shell fossil fragments, and organic matter, 0–1.8 m thick.

Unit 2-2a: A set of deep light-gray silty clay, enriched with shell fossil debris. It is distributed in the four drillings of ZK5-2, ZK5-1, ZK5-9, and ZK5-10, with a thickness range of 0.3–0.4 m, which can be easily identified and used as a marked stratum to judge the fault activity.

Unit 2-2b: The unit strata are distributed in each drilling without ZK5-4. They are dark gray-cyan silt and clay, containing a small amount of shell fragments, 0.3–2.85 m thick.

Unit 2-3a: A set of pale silty sandy clay, clayey sand, containing a small amount of shell debris, 0.2–0.25 m thick, evenly distributed except for ZK5-2 and ZK5-1.

Unit 2-3b: A set of gray-black sandy clay and gravels with distributions in every drilling except for ZK5-2 and ZK5-1, 0.6–2.8 m thick.

Unit 2-4a: In this unit, grayish-brown medium coarse sand, grayish-black clay at ZK5-10, ZK5-7, and ZK5-11, and black decaying wood at the top, 0.2–0.3 cm thick.

Unit 2-4b: Gray silty clay, abundant shell enrichment layer, only ZK5-10, ZK5-7, ZK5-11, ZK5-6 are retained, 0.82–1.4

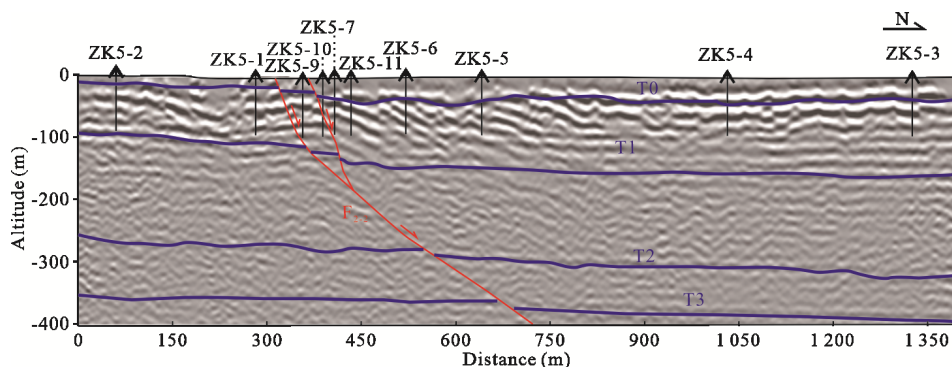


Figure 3. Interpretation of the shallow seismic profile of S142.



Figure 4. Lithologic characteristics of the strata revealed by drillings.

m thick.

Unit 2-5: The unit strata are grayish black silty clay, containing a small amount of shells and fine gravel; only ZK5-10 and ZK5-11 are preserved herein, 1.03–1.2 m thick.

Unit 3: Grayish yellow, grayish white with reddish brown gravel in coarse sand, with a small amount of nodule, it belongs to Pleistocene Basuo Formation and Beihai Formation ( $Qp^3bs$  and  $Qp^2b$ ). However, ZK5-9, ZK5-10, ZK5-7, and ZK5-11 have not been preserved, probably because they were washed away by rivers, 0.2–5.8 m thick.

Unit 4: It is mainly a set of shell-clastic rock and conglomerate interbeds with the sandstone, showing three sedimentary cycles. It belongs to Pliocene Haikou Formation ( $N_1h$ ). It can be divided into six layers as follows.

Unit 4-1: Yellow-brown, blackish-brown sandy clay, 1–5.7 m thick.

Unit 4-2: A light grayish yellow shell-clastic rock with a bioclastic structure and a massive structure comprising detrital and cemented material, 1.3–10.03 m thick.

Unit 4-3: This is the second sedimentary cycle of unit 4 and the thickest subunit, comprising gray-black to gray-green sandy clay, fine medium sandy clay, with half cemented, 33–69.5 m thick. Notably, fault planes and scratches are evidently found at a depth range of 47.24–53.71 m in the ZK5-10 drilling (Figures 5a, 5c). The dip angle of the fault planes was approximately in the range of  $70^\circ$ – $80^\circ$ , and there were evident fault scratches and positive steps on the fault surface. The scratches were strike-like, and the step steep was curved downward, indicating the downward direction of the movement of the opposite plate.

Unit 4-4: Yellow-brown semiconsolidated bioclastic sandstone, 1.7–10.05 m thick.

Unit 4-5: Grey-dark gray with coarse sand in pebbles, containing biotritus, 2.7–20.05 m thick.

Unit 4-6: Maroon conch conglomerate with better cementation, 7.6–12.8 m.

Unit 5: It is a set of gray green medium-fine grained sandstone which belongs to Miocene Denglujiao Formation ( $N_1d$ ), and has not hit the bottom.

### 3.4 Dating Results and Analysis

#### 3.4.1 OSL dating results and analysis

Table 2 presents the OSL dating results. The OSL dating age accords with the law of stratigraphic sequence of lower older and upper younger. The age at the top of ZK5-1-1 is  $6\,600 \pm 500$  a BP, the age of ZK5-6-2 is  $6\,800 \pm 500$  a BP, the age of ZK5-6-6 is  $7\,900 \pm 600$  a BP, and the age of ZK5-7-1 is  $7\,000 \pm 150$  a BP. As shown in Figure 5, the four samples of the interpreted light signal are stronger, with rapid attenuation curve characteristics, which implies a typical quartz signal, thus meeting the requirements of OSL dating. The sample dispersion is between 3.8 and 7.1, and the dating results are reliable.

#### 3.4.2 AMS<sup>14</sup>C dating results and analysis

The AMS<sup>14</sup>C samples were sent to Bata Laboratory in the United States for testing and corrected by tree-ring age comparison (Figure 5). Table 3 presents the results.

From Table 3, we find that the corrected ages of the samples range from 6 568 to 8 980 a BP, which represents the approximate age of strata formation at different altitudes. Among them, the ZK5-5 sample was tested with charcoal and shell at a depth range of 5.6–5.7 m.

The laboratory age of the charcoal in ZK5-5 was  $7\,950 \pm 30$  a BP, the shell age was  $7\,650 \pm 30$  a BP, and their correction ages were 8 980–8 649 and 8 539–8 405 cal BP, respectively, which demonstrates that the charcoal was slightly older than the shell. The ages of the fault zone strata since the Holocene revealed by the drillings are key data for judging the fault distance and determining the latest active age of active faults. Because the error of the OSL result is greater than that of AMS<sup>14</sup>C, we mainly rely on the AMS<sup>14</sup>C results as the stratigraphic age data and the optically luminescent data as supplementary reference. Hence, the age of each set of strata since the Holocene is as follows: U1 age is approximately  $6\,600 \pm 500$  a BP; U2-1 age is  $6\,383$ – $6\,568$  a BP. The age of U2-2 is  $6\,910$ – $7\,955$  a BP, in which the top is  $6\,910$ – $7\,274$  a BP, and the middle and lower part is approximately  $7\,828$ – $7\,955$  a BP. The age of U2-3 is  $6\,910$ – $8\,366$  a BP, in which the top is  $7\,587$ – $7\,676$  a BP, the middle is  $7\,939$ – $8\,019$  a BP, and the bot-

**Table 2** Results of OSL dating

Sample code	Depth (m)	U ( $\mu\text{g/g}$ )	Th ( $\mu\text{g/g}$ )	K (%)	Water content (%)	Environmental dose rate (Gy/ka)	Equivalent dose (Gy)	Age (Ka BP)	Stratigraphical sequence No.
ZK5-1-1	1.1–1.2	$3.35 \pm 0.15$	$13 \pm 0.15$	$1.65 \pm 0.06$	16.8	$3.28 \pm 0.23$	$21.61 \pm 0.41$	$6.6 \pm 0.5$	U1
ZK5-7-1	1.0–1.1	$2 \pm 0.15$	$10.4 \pm 0.15$	$1.37 \pm 0.06$	32.1	$2.11 \pm 0.16$	$14.72 \pm 0.31$	$7.0 \pm 0.15$	U1
ZK5-6-2	3.2–3.3	$2.72 \pm 0.15$	$14.6 \pm 0.15$	$1.8 \pm 0.06$	12.9	$3.43 \pm 0.24$	$23.23 \pm 0.47$	$6.8 \pm 0.5$	U2-2b
ZK5-6-6	7.4–7.5	$3.93 \pm 0.15$	$17.3 \pm 0.15$	$1.71 \pm 0.06$	20.8	$3.63 \pm 0.29$	$28.74 \pm 0.36$	$7.9 \pm 0.6$	U2-4b

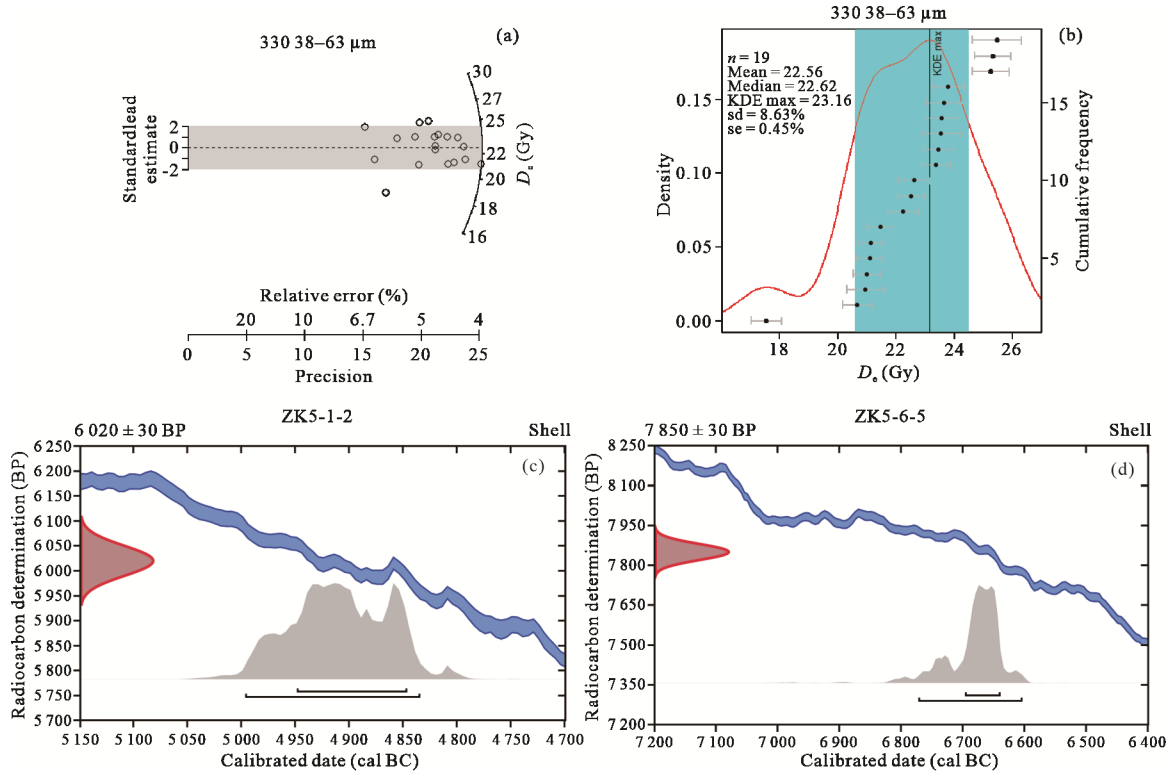


**Figure 5.** Representative sample testing analysis results. (a) Radial plot distribution of ZK5-6-2; (b) distribution of kernel density estimates of ZK5-6-2; (c) calibrated radiocarbon age curves of ZK5-1-2; (d) calibrated radiocarbon age curves of ZK5-6-5.

tom is 8 200–8 366 a BP. The middle part of the U2-4 is 8 554–8 722 a BP, the bottom part is 8 695–9 006 a BP, and the age of U2-5 is 8 746–9 090 a BP.

## 4 DISCUSSION

### 4.1 Holocene Activities in the MPF Middle Segment

#### 4.1.1 Fault identification and property judgment

Based on the location of the top breakpoint and the vertical displacement of the fault revealed by shallow seismic profile detection and drillings, we conclude that there are two faults (F2-2' and F2-2'') on the profile line (Figure 6). A geomorphologic survey shows that the faults cut through the Holocene deposition and formed a fault sag pool (Figure 2c). Combined with the drainage deflection phenomenon (Figure 2d) and stratigraphic age results, we deduce that the two faults are all Holocene normal faults and may be combined with a right-lateral strike-slip. F2-2' is between ZK5-1 and ZK5-7 (Figure 6). The geological profile across the fault and the fault plane of ZK5-1 0 (Figure 5c) show that the F2-2'' is between ZK5-9 and ZK5-7, which passes through ZK5-10. And the scratch characteristics (Figure 5c) also show that the normal faults should be

combined with a right-lateral strike-slip.

#### 4.1.2 Fault activity history and velocity

Fault activity is an important factor in evaluating earthquake risk and crustal stability. Most of the faults in the MPF zone are buried. Their magnitude and the latest age of the fault activity need to be analyzed based on the strata and ages revealed by the drillings. Before calculating the fault displacement, it is necessary to determine the marked strata formed by horizontal deposition. Based on the stratigraphic characteristics of the seismic zone area described in Section 4.3, the bottoms of U1, U2-1, U2-2, U2-3, U3, and U-4 are selected as the marked strata of fault dislocation.

Table 4 presents the results calculated from the strata ages and marked horizon elevations. The F2-2' is a normal fault, dipped to the north, and cutting through the surface. The bottoms of U1, U2-2, U3, and U4 are offset by 1.05, 1.51, 0.8, and 3.5 m, respectively, and the fault activity rate is 2.32 mm/a since 6 500 a BP. The F2-2'' is also a normal fault, dipping to the north, and cutting through the surface. The bottoms of U1, U2-1, U2-2, U2-3, and U4 are offset by 0.33, 1.35, 1.91, 1.88,



**Table 3** Results of  $^{14}\text{C}$  dating

Sample No.	Depth (m)	Sample material	Measured radiocarbon age (a BP)	Conventional radiocarbon age (cal BP)	Stratigraphical sequence No.
ZK5-9-2	1.8	Shell	6 050 ± 30	6 568–6 383	U2-1
ZK5-1-2	1.1–1.2	Shell	6 020 ± 30	6 947–6 785	U2-2a
ZK5-2-1	1.25–1.4	Shell	6 420 ± 30	7 421–7 280	U2-2a
ZK5-9-3	2.5	Shell	6 500 ± 30	7 130–6 910	U2-2a
ZK5-10-2	3.5	Shell	6 670 ± 30	7 274–7 138	U2-2a
ZK5-11-2	2.41	Shell	6 540 ± 30	7 151–6 959	U2-2b
ZK5-6-4	4.8	Shell	7 050 ± 30	7 955–7 828	U2-3a
ZK5-7-3	5.8–6.0	Shell	7 160 ± 30	8 019–7 939	U2-3a
ZK5-9-5-2	4.4	Wood charcoal	6 790 ± 30	7 676–7 587	U2-3a
ZK5-10-5	6.5	Shell	7 160 ± 30	7 690–7 561	U2-3a
ZK5-11-3	4.54	Shell	6 970 ± 45	7 691–7 873	U2-3a
ZK5-5-2	5.6	Wood charcoal	7 950 ± 30	8 980–8 649	U2-4a
ZK5-5-3	5.6–5.7	Shell	7 670 ± 30	8 539–8 405	U2-4a
ZK5-6-5	6.1	Shell	7 850 ± 30	8 722–8 554	U2-4a
ZK5-7-4	7.8–8.0	Shell	7 890 ± 30	8 780–8 593	U2-4a
ZK5-11-5	9.4	Shell	7 985 ± 50	8 695–9 006	U2-4b
ZK5-11-6	11.1	Shell	8 050 ± 50	8 746–9 090	U2-4b

**Table 4** Fault F2-2 activity and velocity at the middle section of the MPF

Fault No.	F2-2'						F2-2''					
Dip	N											
Formation No. offset by the fault	U1	U2-1	U2-2	U2-3	U3	U4	U1	U2-1	U2-2	U2-3	U4	
Elevation of the footwall top boundary (m)	Surface	--	1.36	--	-0.75	-5.74	Surface	0.31	-0.42	-2.3	-6.54	
Age of the footwall top boundary formation (a)	--	6 420 ± 30	6 020 ± 30	--	--	--	--	6 050 ± 30	6 050 ± 30	6 790 ± 30	--	
Elevation of the footwall bottom boundary (m)	1.36	--	-0.79	--	-5.74	-88.34	0.31	-0.42	-2.3	-4.54	-91.84	
Age of the footwall top boundary formation (a)	6 600 ± 500	--	--	--	--	--	--	--	6 500 ± 30	--	--	
Elevation of the hanging wall top boundary (m)	Surface	0.31	-0.42	-2.3	-4.54	-6.54	Surface	-0.02	-0.93	-4.21	-7.82	
Age of the hanging wall top boundary formation (a)	--	--	6 050 ± 30	6 790 ± 30	--	--	--	--	6 670 ± 30	7 160 ± 30	--	
Elevation of the hanging wall bottom boundary (m)	0.31	-0.42	-2.3	-4.54	-6.54	-91.84	-0.02	0.93	-4.21	-6.42	-96.1	
Age of the hanging wall top boundary formation (a)	--	--	6 500 ± 30	--	--	--	--	--	6 800 ± 500	7 470 ± 30	--	
Fault displacement (m)	1.05	--	1.51	--	0.8	3.5	0.33	1.35	1.91	1.88	4.26	
Fault nature	Normal fault with a dextral strike-slip						Normal fault with a dextral strike-slip					
Fault vertical displacement rate	2.32 mm/a (from 6 500 a)						2.5 mm/a (from 7 470 a)					

and 4.26 m, respectively, and the fault activity rate is 2.5 mm/a since 7 470 a BP. It's worth noting that the offset value sequences should show increasing downward from top to bottom if stratigraphic denudation had not occurred. In our work, the U2-3 to U3 stratum shows smaller offset value than the real offset value as it is denuded during the last deglaciation after the fault activity.

The activity history of the fault can be recovered based on the faults of different marked strata from bottom to top. As shown in Figures 6a and 7, F2-2 has experienced at least five stages of activities. The first stage occurred after the sedimentary completion of U5 in the Miocene Denglujiao Formation ( $N_1d$ ) and before the sedimentary completion of U4 in the Pliocene Haikou Formation ( $N_2h$ ). The fault distances of F2-2' and

F2-2'' are more than 2.7 and 2.38 m, respectively. The second stage occurred after the deposition of the Pliocene Haikou Formation ( $N_2h$ ) and before the deposition of U3 in the Early–Middle Quaternary. Considering that the U3 formation was denuded, the fault distances of F2-2' and F2-2'' are more than 0.46 and 0.56 m, respectively. The third stage occurred after the deposition of U3 and before the deposition of U2-1. Due to the denudation of U3 and early U2 strata, the displacement value of F2-2' activity should be greater than 0.56 m. The fourth stage occurred after U2-1 deposition and before U1 deposition, with the fault spacing being more than 0.46 m. The F2-2'' fault spacing is 1.02 m. The fifth stage occurred after U1 deposition. The fault spacing is 1.05 m, and the F2-2'' fault spacing is 0.33 m.

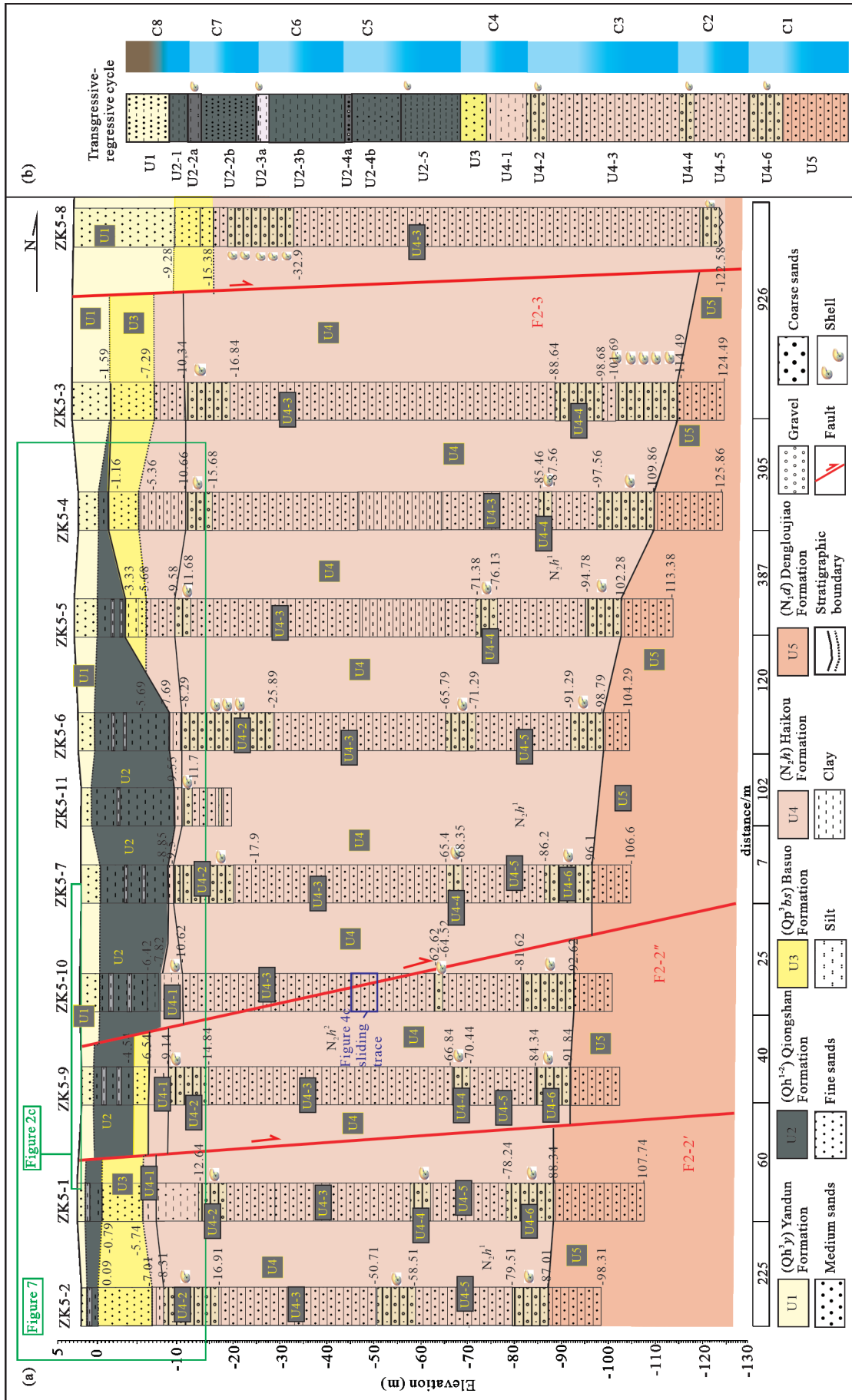


Figure 6. Geological profile across the fault and correlation with the marine transgressive-regressive. (a) Geological profile across the fault revealed by drillings; (b) schematic of the relationship between marine transgressive-regressive cycle and stratigraphic deposition in the study area.

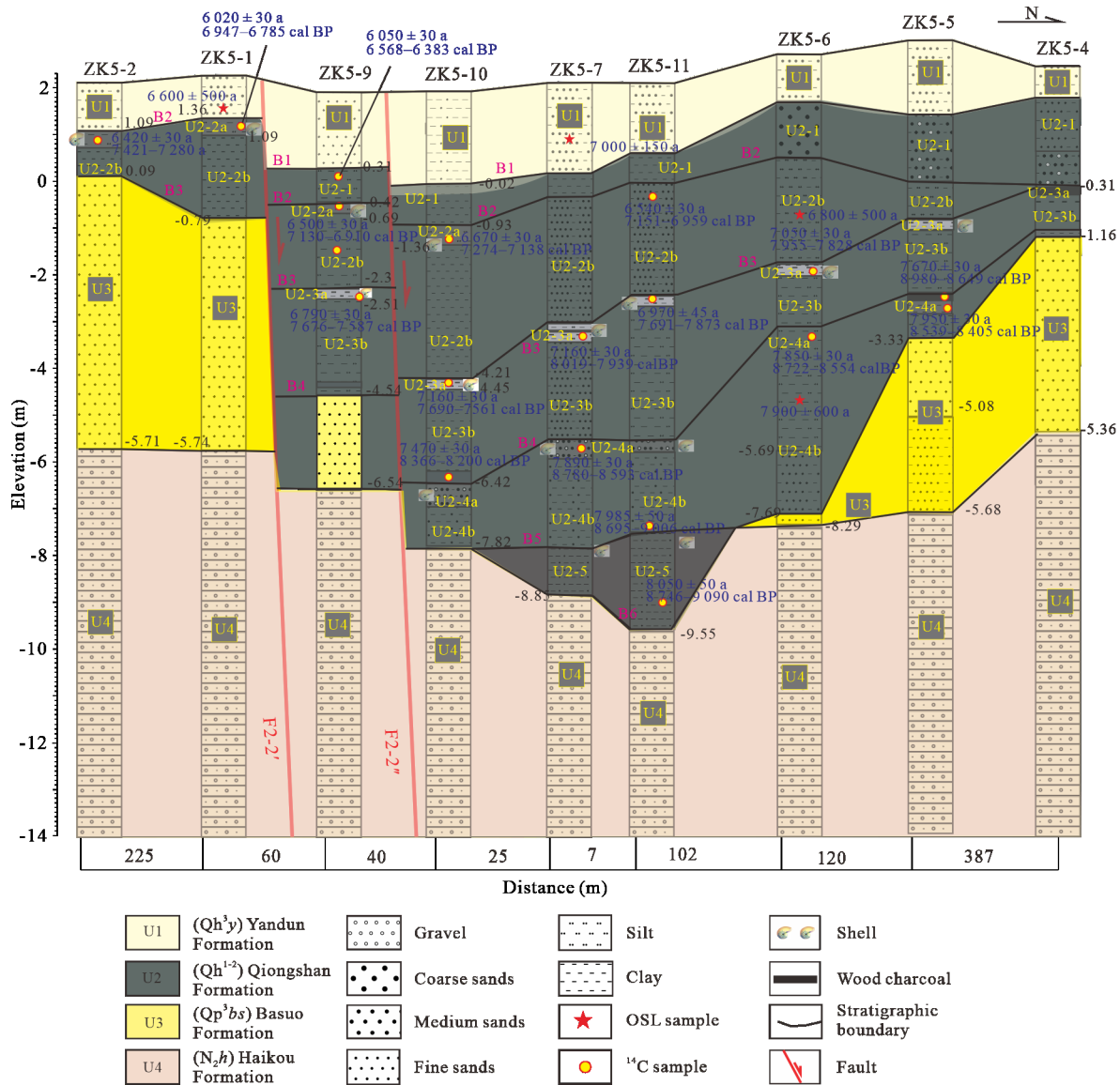


Figure 7. Diagrams showing the detailed enlargement Holocene geological profile across the fault revealed by drillings.

## 4.2 Tectonics and Climate Response of Stratigraphic Development in the Epicenter Area of 1605 Qiongzhan M7½ Earthquake since Late Cenozoic

### 4.2.1 Marine transgression-regression cycles reflected by sedimentation

The MPF zone is located in the coastal belt where stratigraphic development environment is complex because of the influences of climate change, marine transgression-regression, tectonic and volcanic eruption.

Based on the stratigraphic sequence introduced in Figure 6a and Section 4.3, we find that there were eight cycles of marine transgression and regression since the Miocene. The Denglujiao Formation (N<sub>1</sub><sup>d</sup>) (U5) formed during the Miocene is a set of grayish green medium fine sand, which represents a marine sedimentary environment. U4-6, U4-4, and U4-2 belonging to the Haikou Formation (N<sub>2</sub><sup>h</sup>) are three sets of coastal environment shell sand conglomerate, representing three marine regression stages. U4-5, U4-3, and U4-1 are marine gray-green clay and medium-fine sand, representing the sedimentary envi-

ronment occupied by the ocean in the study area. U3 is a set of terrestrial sedimentary sand and gravel layers deposited in the Pleistocene. The thickness of U3 is thinner than other units owing to the crust uplift in most of the Pleistocene. U2-5 and U2-4b are a set of marine bluish silty clay, clayey sand, containing shells. U2-4a is a set of gray and black sandy clay and sand and gravels of marine and continental transitional facies. Charcoal developed in mangroves contains a large number of shell enrichment layers. U2-3b is a set of marine medium coarse sand, and U2-3a is a set of marine and continental transitional clayey sand, containing a large number of shell enriched layers. U2-1 is a marine silty clay, medium fine and coarse sand, while U1 is a set of terrestrial medium fine sand. The U2 and U1 are drowned valley and marine deposits in the high sea level period of transgression period of late glacial period and early and middle glacial period.

Based on a comparison of sea level changes in the northern part of the South China Sea, (Xie et al., 2012), the sedimentary environment of multiple periods of marine transgressions and



regressions in this area since the Miocene was restored. During the Miocene ( $N_1$ ), this area was still a vast ocean. In the Early Pliocene, approximately 5.2–4.3 Ma BP, the area retreated into a coastal environment, and the U4-6 shell glutenite was deposited. During  $\sim(4.3\text{--}3.9)$  Ma BP, the sea level rose in the South China Sea, and the gray-green marine silty clay and medium-fine sand of U4-5 were deposited. During approximately 3.9–3.3 Ma BP, the sea level dropped again, and the northern Hainan Island area changed from ocean to coastal zone, and a set of shell sand conglomerate of U4-4 was deposited. After 3.3–3.2 Ma BP, the sea level rose, leading to the deposition of fine sand and sandy clay in the gray-green marine facies of U4-3. During  $\sim(3\text{--}2.7)$  Ma BP, the sea level fell to the coastal zone, and a set of shell glutenite of U4-1 was deposited. During  $\sim(2.6\text{--}2.5)$  Ma BP, the sea level rose again, and a clay layer of U4-1 was deposited. In the Early Pleistocene of the Quaternary period, the sea level began to decline, and many lakes appeared in the northern Hainan Island, and a set of coastal plain facies clay and fine sand of U3 were deposited. During the early Pleistocene, the crust was relatively uplifted, and rivers developed. In the Middle Pleistocene, the strata were denuded, and the volcanic eruption formed the basalts of the Duowen Formation ( $Qp^2d$ ). During the period of high sea level in the Holocene,  $\sim(8\ 000\text{--}5\ 000)$  a BP, a set of gray and gray black sandy clay and clay sand deposits of U2 was developed, which experienced four small cycles of marine-land transition in the middle segment of the MPF zone by the fault activity and climate changes (Figure 6b). In the period of sea retreat, a large number of shell enrichment layers were deposited along the seashore in the study area. Around  $\sim 6\ 500$  a BP, the study area was once again exposed as land.

#### 4.2.2 Tectono-sedimentary response

As shown in Figure 6a, because of the activity effect of F2-3, the top layer of the Denglou Jiao Formation (U5) in the Miocene gradually decreased from south to north. In the Pliocene, the Beihai Formation (U4) gradually thickened to the north due to the syndeposition of the descending hanging wall of F2-2. The strata were more significantly affected by fault activities since the Quaternary. Due to the F2-2 activity, the hanging wall of the fault kept falling and became a valley in the terrain. As a result, the U3 strata in central ZK5-10, ZK5-7, and ZK5-11 were denuded by river or sea and were not preserved during the last deglaciation (Figure 7). At the same time, the fault activity resulted in the thickening of the Holocene strata with a slight dip to the south on the hanging wall, showing V-shaped characteristics (Figure 7).

#### 4.2.3 Controlling effect of the MPF on the Qiongsan earthquake of 1605

The 1605 Qiongsan  $M7\frac{1}{2}$  Earthquake in Haikou, Hainan Island was the most destructive earthquake in the northern continental margin of the South China Sea (Xu, 2007; Chen and Huang, 1989). As to the source seismogenic fault of this earthquake, there is still no clear understanding (Wang et al., 2021; Li W et al., 2019; Liu F X et al., 2018; Liu H G et al., 2018; Xu, 2007, 1986a, b, c, 1985; Li P et al., 1988).

Based on the analysis of recently found evidence, the MPF may be the seismogenic fault of the Qiongsan Earthquake for

three reasons. First, large earthquakes often occur along long fault lines (Deng et al., 2001). In terms of the length of fault development, the NW PQF (F13), which is only 20–25 km away, has clear evidence of activity, mainly distributed in Dongzhai Port and Qiongzhou Strait to the north of Sanjiang River, and no evidence of its extension or activity can be found to the south. The MPF is a successor fault that has been active since the Miocene. The length of the fault is proven to be approximately 132 km since the Late Pleistocene in the North Qiongsan area, and it may extend to the west. Second, the MPF is an active fault that can trigger large earthquakes. Based on the distribution of large earthquakes recorded throughout history, the MPF zone has not only experienced an  $M7\frac{1}{2}$  earthquake in 1605, but also a  $M5$  earthquake in 1913 and an  $M7\frac{1}{2}$  earthquake in 1618 (Figure 1). Third, based on the activity of the fault in the middle segment of the MPF in this study, where the epicenter of the 1605 Qiongsan  $M7\frac{1}{2}$  Earthquake was located, it can be seen that there have been five activities since the Late Miocene, and the fault has cut through the latest surface strata and caused landform water to form a pool. These results indicate that the MPF should have been active more than 400 years ago. It may very well be the major seismogenic fault that caused the 1605  $M7\frac{1}{2}$  earthquake. Attention should be paid to this fault activity risk in the urban development planning of Hainan Island.

## 5 CONCLUSIONS

(1) The middle segment of the MPF, which was the epicenter of the 1605 Qiongsan  $M7\frac{1}{2}$  Earthquake, is composed of three nearly parallel normal faults: “Macun-Luodou fault (F2-1), Haixiu-Dongyuan fault (F2-2), and Changliu-Zhuxihe fault (F2-3)”. We conducted a detailed study on F2-2. The results show that F2-2 is composed of two secondary faults, namely F2-2' and F2-2'', with a flower-shaped structure buried under the ground; it is distributed nearly east-west and dips to the north. The occurrence above 100 m depth is  $\sim 70^\circ$  shallow and steep, and the occurrence gradually subsides at depths below 100 m depth. Based on the deformation of the geomorphology and drainage system, the fault may also have a dextral strike-slip. F2-2 has experienced at least five stages of activities since the Miocene. The vertical activity rates of F2-2' and F2-2'' are  $\sim 2.32$  and  $\sim 2.5$  mm/a, respectively, since the Holocene.

(2) The sedimentary environment of multiple periods of marine transgressions and regressions in this area and tectono-sedimentary response since the Miocene was restored. There were eight cycles of marine transgression and regression since the Miocene. The top layer of the Dengloujiao Formation ( $N_1d/U5$ ) in the Miocene gradually decreased from south to north, due to the effect of F2-3 activity. The F2-2 activity resulted in the thickening of the Holocene strata with a slight dip to the south on the hanging wall, showing V-shaped characteristics.

(3) Based on the development length of the fault, the distribution of major earthquakes throughout history, and the latest stratigraphic structure cut by the fault, we can conclude that the MPF is the source seismogenic fault of the 1605 Qiongsan  $M7\frac{1}{2}$  Earthquake.

## ACKNOWLEDGMENTS

The authors thank the reviewers for their valuable com-

ments and suggestions on this manuscript. Thanks also go to Associate Professors Limin Wang and Linsong Wang from the School of Geophysics and Geomatics, China University of Geosciences, Wuhan for the processing and interpretation of shallow seismic profiles. This study was financially supported by the National Natural Science Foundation of China (No. 42272222), the Basic Research Funds of Institute of Geomechanics, Chinese Academy of Geological Sciences (No. DZLXJK202211), and China Geological Survey (Nos. DD20190306, DD20190546, DD20160269, DD20230249). The final publication is available at Springer via <https://doi.org/10.1007/s12583-021-1585-x>.

### Conflict of Interest

The authors declare that they have no conflict of interest.

### REFERENCES CITED

- Chen, E. M., Huang, Y. Y., 1979. Preliminary Discussion on the 1605 Qiongzhou Earthquake and Its Seismogenetic Structure. *Seismology and Geology*, 1(4): 37–44, 99–100 (in Chinese with English Abstract)
- Chen, E. M., Huang, Y. Y., 1989. Characteristics of the Seismic Damage and Analysis of the Seismic Structure of the 1605 Great Earthquake of Qiongzhou, Hainan Island. *Acta Seismologica Sinica*, 11(3): 319–331 (in Chinese with English Abstract)
- Chen, J. J., Leng, C. B., Fu, L. B., et al., 2024. Genesis of Delong Granite in East Kunlun Orogen and Its Implication on the Evolution of Paleotethys Ocean. *Earth Science*, 49(2): 560–576. <https://doi.org/10.3799/dqkx.2022.328> (in Chinese with English Abstract)
- Deng, Q. D., Wang, Y. P., Zhang, P. Z., 2001. Research on Active Fault 8. Seismological Press, Beijing (in Chinese with English Abstract)
- Ding, Y. Z., 1988. A Collection of Earthquake Studies in Northern Hainan Island. Seismological Press, Beijing (in Chinese with English Abstract)
- Fan, Q. C., Sun, Q., Li, N., et al., 2004. Periods of Volcanic Activity and Magma Evolution of Holocene in North Hainan Island. *Acta Petrologica Sinica*, 20(3): 533–544 (in Chinese with English Abstract)
- Geological Survey Institute of Hainan Province, 2019. Regional Geology of Hainan Province. Geological Publishing House, Beijing (in Chinese)
- Hu, D. G., Ma, X. M., Jia, L. Y., et al., 2019. Investigation of Active Faults and Evaluation of Crustal Stability in Pan Pearl River Delta. CGS Project Report, Institute of Geomechanics, Chinese Academy of Geological Sciences, Beijing, 28–73 (in Chinese with English Abstract)
- Hu, Y. X., Hao, M., Ji, L. Y., et al., 2016. Three-Dimensional Crustal Movement and the Activities of Earthquakes, Volcanoes and Faults in Hainan Island, China. *Geodesy and Geodynamics*, 7(4): 284–294. <https://doi.org/10.1016/j.geog.2016.05.008>
- Huang, Z. G., Cai, F. X., 1994. A New Approach to the Quaternary Volcanicity in the Leiqiong Area. *Tropical Geography*, 14(1): 1–10 (in Chinese with English Abstract)
- Jia, S. X., Li, Z. X., Xu, Z. F., et al., 2006. Crustal Structure Features of the Leiqiong Depression in Hainan Province. *Chinese Journal of Geophysics*, 49(5): 1385–1394 (in Chinese with English Abstract)
- Li, F. R., Xiong, F. H., Ma, C. Q., et al., 2024. Petrogenesis of Triassic Hongshuihe Granitoids in East Kunlun: Implications for the Paleotethyan Orogeny. *Earth Science*, 49(2): 639–655. <https://doi.org/10.3799/dqkx.2022.165> (in Chinese with English Abstract)
- Li, J. H., Zhang, Y. Q., Dong, S. W., et al., 2012. Late Mesozoic–Early Cenozoic Deformation History of the Yuanma Basin, Central South China. *Tectonophysics*, 570: 163–183. <https://doi.org/10.1016/j.tecto.2012.08.012>
- Li, P., Yang, M. E., Liu, X. S., et al., 1988. A Collection of Earthquake Studies in Northern Hainan Island. Seismological Press, Beijing, 41–52 (in Chinese with English Abstract)
- Li, W., Jia, L. Y., Hu, D. G., et al., 2019. Late Pleistocene Tectonic History of the Western Segment of Maniao-Puqian Fault: Evidence from the Laocheng Section, Northern Hainan Island. *Geoscience*, 33(5): 970–978 (in Chinese with English Abstract)
- Li, Z. X., Zhao, W. J., Liu, G. X., 2006. A Study on Deep Crust Structures and Stress Situation of the 1605 Qiongzhou Strong Earthquake. *South China Journal of Seismology*, 26(1): 28–36 (in Chinese with English Abstract)
- Lin, Z. Y., Hu, H. X., Zhu, L. B., et al., 1988. Preliminary Results of Crustal Structure Study in Leiqiong Area. In: A Collection of Earthquake Studies in Northern Hainan Island. Seismological Press, Beijing, 127–139 (in Chinese with English Abstract)
- Liu, F. X., Miao, Y. Y., Jing, Z. J., et al., 2018. Late Pleistocene Activities Characteristics of Western Segment of Puqian-Qinglan Fault. *Global Geology*, 37(1): 148–153 (in Chinese with English Abstract)
- Liu, H. G., Li, F., Jia, Q. C., 2018. Activity Discussion of the Western Segment of the Maniao-Puqian Fault Revealed by Drilling. *South China Journal of Seismology*, 38(1): 47–53 (in Chinese with English Abstract)
- Liu, H., Hong, H. J., Ran, H. L., et al., 2008. Dynamic Mechanism of Volcanic Belt and New Understanding from Earthquake Evidence in Northern Hainan Island, China. *Chinese Journal of Geophysics*, 51(6): 1804–1809 (in Chinese with English Abstract)
- Liu, Y., Hu, D. G., Xu, S. F., et al., 2020. Electrical Anisotropic Structure in the Quaternary Volcanic Region of North Hainan Island and Its Geological Implications. *Earth Science*, 45(1): 330–340. <https://doi.org/10.3799/dqkx.2018.336> (in Chinese with English Abstract)
- Long, H. G., Lin, Y. H., Zhu, Y. H., et al., 2006. Establishment of the Early–Mid Pleistocene Duowen Formation on Northern Hainan Island, China. *Geological Bulletin of China*, 25(3): 408–414 (in Chinese with English Abstract)
- Peng, X., Li, C. F., Song, T. R., et al., 2022. Deep Structures and Lithospheric Breakup Processes at Northern Continent–Ocean Transition Zone of the South China Sea. *Earth Science*, 47(11): 4245–4255. <https://doi.org/10.3799/dqkx.2022.366> (in Chinese with English Abstract)
- Ren, Z. H., He, X. L., 2006. Discussion on the Location of the ‘Aftershocks’ of the Macroquake Occurred in 1605 from the Point of View of Active Tectonics. *South China Journal of Seismology*, 26(1): 9–16 (in Chinese with English Abstract)
- Sun, J. Z., Yan, F. H., 1988. Study on Quaternary Stratigraphic Chronology in Northern Hainan. A Collection of Earthquake Studies in Northern Hainan Island. Seismological Press, Beijing, 17–25 (in Chinese with English Abstract)
- Wang, C. Q., Jia, L. Y., Hu, D. G., et al., 2021. Activity Characteristics of the Eastern Maniao-Puqian Fault, Northern Hainan Island and Its Evaluation of Crustal Stability. *Geology in China*, 48(2): 618–631 (in Chinese with English Abstract)
- Wang, H. J., 1981. Division of Cenozoic Strata in Leiqiong Area, Guangdong Province. *Journal of Stratigraphy*, 5(3): 221–225 (in Chinese)
- Xia, M. M., Wang, C. Q., Hu, D. G., et al., 2019. ESR Dating of the Basuo Formation in the Northeastern Hainan Island and Its Tectonic Significance. *Journal of Geomechanics*, 25(2): 257–266 (in Chinese with English Abstract)
- Xu, Q. H., 1985. Discussion on Subsidence Mechanism of Qiongzhou

- Earthquake. *South China Journal of Seismology*, 5(4): 33–40 (in Chinese with English Abstract)
- Xu, Q. H., 1986a. Recent Sinking in the Dongzhai Harbour Area, Northern Qiongzhou. *Marine Sciences*, 10(1): 24–28 (in Chinese with English Abstract)
- Xu, Q. H., 1986b. An Understanding of Seismic Geology in Lei Qiong Depression. *South China Journal of Seismology*, 6(1): 83–93 (in Chinese with English Abstract)
- Xu, Q. H., 1986c. Formation and Migration of Dongzhai Port in the Northern Hainan Island and the Major Qiongzhou Earthquake of 1605. *Seismology and Geology*, 8(3): 92–96 (in Chinese with English Abstract)
- Xu, Q. H., 2007. The Land Sank into the Sea and Possible Tsunami by the Great Earthquake in Qiongzhou in China in 1605. *Acta Oceanologica Sinica*, 29(3): 146–156 (in Chinese with English Abstract)
- Xu, S. C., Gao, X. K., Li, H. Y., 1982. Large Area Subsidence may be Evidence of Phase Change in Source Region—Preliminary Study on the Genesis of Qiongzhou Earthquake. *South China Journal of Seismology*, 2(1): 3–7 (in Chinese with English Abstract)
- Xu, X. W., 2015. An Introduction to Urban Active Faults in China. Seismological Press, Beijing. 380–403 (in Chinese with English Abstract)
- Xue, W. J., 1983. On the Age and Sedimentation Environment of Beihai Formation. *Marine Geology & Quaternary Geology*, 3(3): 35–52 (in Chinese with English Abstract)
- Yang, M. E., Li, P., Dou, Y. Q., 1988. Discussion on the Relationship between Quaternary Volcanic Activity and Fault Activity in Qiongzhou Area. In: A Collection of Earthquake Studies in Northern Hainan Island. Seismological Press, Beijing. 63–71 (in Chinese with English Abstract)
- Zhang, G. W., Guo, A. L., Wang, Y. J., et al., 2013. Tectonics of South China Continent and Its Implications. *Science China Earth Sciences*, 56(11): 1804–1828. <https://doi.org/10.1007/s11430-013-4679-1>
- Zhang, Y. M., Zhang, R. J., Yao, H. Z., et al., 1997. The Precambrian Crustal Tectonic Evolution in Hainan Island. *Earth Science—Journal of China University of Geosciences*, 22(4): 395–400 (in Chinese with English Abstract)
- Zhao, Y. H., Tong, D. J., Song, Y., et al., 2016. Seismic Reflection Characteristics and Evolution of Intrusions in the Qiongdongnan Basin: Implications for the Rifting of the South China Sea. *Journal of Earth Science*, 27(4): 642–653. <https://doi.org/10.1007/s12583-016-0708-2>
- Zhou, Y., Zhao, Y. S., Cai, Y. F., et al., 2023. Permian-Triassic Magmatism in the Qin-Fang Tectonic Belt, SW China: New Insights into Tectonic Evolution of the Eastern Paleo-Tethys. *Journal of Earth Science*, 34(6): 1704–1716. <https://doi.org/10.1007/s12583-020-1111-6>